Critical analysis of the reentrant localization transition in a one-dimensional dimerized quasiperiodic lattice

Shilpi Roy,[1] Sourav Chattopadhyay,[1,2] Tapan Mishra,[1] and Saurabh Basu[1]

[1]*Department of Physics, Indian Institute of Technology Guwahati-Guwahati, Assam 781039, India*
[2]*Department of Physics, ICFAI University, Tripura, West Tripura 799210, India*

A reentrant localization transition was predicted recently in a one-dimensional quasiperiodic lattice with dimerized hopping between the nearest-neighbor sites [Roy *et al.*, Phys. Rev. Lett. **126**, 106803 (2021)]. It was shown that the interplay between the hopping dimerization and a staggered quasiperiodic disorder manifests two localization transitions through two intermediate phases, resulting in four critical points as a function of the quasiperiodic potential. In this paper, we study the critical nature of the states across the localization transitions by computing the mass exponents and the corresponding fractal dimensions of the states through a multifractal analysis. Moreover, we analyze the phenomenon of this reentrant localization transition by examining the spectral properties of the eigenstates. By performing a systematic finite-size scaling analysis for a fixed value of the hopping dimerization, we obtain accurate critical disorder strengths for different transitions and the associated critical exponents. Further, we complement the critical nature of the energy spectrum by computing the Hausdorff dimensions.

I. INTRODUCTION

Anderson localization is a ubiquitous phenomenon in condensed matter that involves lattices with random on-site disorder [1]. The phenomenon, which is marked by the transition of all the extended/delocalized single-particle states to localized states at a critical disorder strength, is absent in one and two dimensions [2]. However, an intermediate between periodic and fully disordered systems, namely, the quasiperiodic lattice, exhibits localization transitions in low dimensions [3]. This remarkable property of quasiperiodic lattices has encouraged the study of localization transitions in various different models [4–8]. Due to the easier experimental access over random lattices, quasiperiodic lattices have been created and studied in different experimental setups such as in optical lattices, photonic lattices, optical cavities, superconducting circuits, etc. [9–12]. These developments have facilitated observations of interesting physical phenomena such as Anderson localization [13–16], Bose glasses [17–21], the emergence of long-range periodic order [22,23], and many-body localization [24–26].

Among the various quasiperiodic lattice models, the simplest interesting model is the Aubry-André (AA) model [8], which exhibits a sharp localization transition. The transition occurs at an exact critical value of the quasiperiodic potential due to the self-dual nature of the AA model [6,8,27]. The sharp localization transition dictates the absence of any energy-dependent mobility edge (ME; the critical energy which separates the localized and delocalized states) at the transition. Hence, the system undergoes a transition from all states extended to all states localized through the critical point. However, the breaking of the self-duality of the AA model

or further generalizations of it have exhibited the localization transition through intermediate/critical regions hosting the ME, e.g., zigzag lattices [28], flat-band lattices [29], quasiperiodic mosaic lattices [30], shallow bichromatic potentials [31], lattices with longer-range hopping [32], and the generalized AA model [33–39]. Furthermore, quasiperiodic lattices exhibit a plethora of unique characteristics, including critical spectra, multifractal wave functions at and away from the critical points corresponding to the localization transition, and the existence of mixed phases hosting the likes of both localized and delocalized states, which have been studied in great detail in various systems [6,31,32,40–48].

Recently, in the context of quasiperiodic lattices, a reentrant localization transition was predicted by some of us in Ref. [49]. It was shown that a one-dimensional quasiperiodic model of AA type with dimerized hopping and staggered quasiperiodic disorder can undergo two localization transitions at the single-particle level. In other words, for some specific dimerization strengths and as a function of disorder, the system first undergoes a localization transition where all the single-particle states get localized. A further increase in the disorder strength makes some of the localized states extended, and eventually, the system undergoes another localization transition at a larger disorder strength where all the single-particle states get localized for the second time. Both localization transitions are found to occur through two intermediate regions hosting the MEs, resulting in four critical points as a function of the quasiperiodic potential strength. While the detailed phase diagram depicting the reentrant localization transition associated with this model was discussed in Ref. [49], a thorough understanding of the phase transitions can be unveiled via a quantitative analysis

of the critical properties, which is relevant and of topical interest.

In this paper, we study the critical properties of the reentrant localization transition described above. By using appropriate finite-size scaling analysis, we explore the critical points associated with different transition types, that is, an extended-intermediate-localized-intermediate-localized transition, as a function of the strength of the quasiperiodic disorder. While from our analysis we are able to obtain the critical points, critical exponents, and scaling behavior associated with the first localization transition, that is, the extended-intermediate-localized-intermediate transition, at the second localization transition, the scaling behavior is not well captured. We further analyze the eigenspectra near the localization transitions and find the existence of multifractal states and identify the critical regimes.

The remainder of this paper is organized as follows. First, we describe the model that exhibits the reentrant localization transition and the approach in detail in Sec. II. In Sec. III, we discuss our main results, which included the multifractal analysis and the critical state analysis. Finally, in Sec. IV we provide a brief conclusion.

II. MODEL AND APPROACH

The Hamiltonian with hopping dimerization and staggered quasiperiodic disorder on a one-dimensional chain is written as [49]

$$
\begin{aligned}
H_{\text{DIM}} = &-t_1 \sum_{n=1}^{N} (\hat{c}_{n,B}^{\dagger} \hat{c}_{n,A} + \text{H.c.}) \\
&- t_2 \sum_{n=1}^{N-1} (\hat{c}_{n+1,A}^{\dagger} \hat{c}_{n,B} + \text{H.c.}) \\
&+ \sum_{n=1}^{N} \lambda_A \hat{n}_{n,A} \cos[2\pi\beta(2n-1) + \theta] \\
&+ \sum_{n=1}^{N} \lambda_B \hat{n}_{n,B} \cos[2\pi\beta(2n) + \theta],
\end{aligned} \tag{1}
$$

where $L = 2N$, with N being the number of unit cells that are denoted by the index n and L is the total system size. Here, a unit cell comprises two sublattice sites, namely, A and B, and the corresponding creation (annihilation) operators are denoted $\hat{c}_{n,A}^{\dagger}$ ($\hat{c}_{n,A}$) and $\hat{c}_{n,B}^{\dagger}$ ($\hat{c}_{n,B}$), respectively. $\hat{n}_{n,A}$ and $\hat{n}_{n,B}$ are the number operators at the two sublattice sites. The intercell hopping between the two sublattices is denoted by t_2, and t_1 refers to the intracell hopping. The hopping dimerization is introduced by defining $\delta = t_2/t_1$ and setting $\delta \neq 1$. We have taken t_1 as the unit of energy throughout the study. The on-site quasiperiodic potential at sublattice site A (B) is given by λ_A (λ_B). The quasiperiodicity is achieved by considering an irrational β. In particular, we take it to be the inverse of the golden mean, namely, $\beta = \frac{(\sqrt{5}-1)}{2}$ [42]. θ denotes the phase difference between the lattices that form the quasiperiodic lattice. In our studies, we consider very large system sizes L up to a maximum of 35 422 sites for which θ can be set to zero without any loss of generality.

Since the primary focus of our studies lies in the critical state analysis and the spectral properties of the model shown in Eq. (1), in the following we outline the details of the approach. In this context, a single-particle state can be written as an eigenstate $|m\rangle$ corresponding to the eigenspectrum E_m of H_{DIM} as

$$
|\psi\rangle = \sum_{i=1}^{L} \phi_i^{(m)} |m\rangle, \tag{2}
$$

where ϕ_i^m defines the probability amplitude corresponding to a lattice site i and m denotes the eigenstate index. An overall understanding of the physical properties of the system can be achieved just by studying the eigenstate $|\psi\rangle$ and eigenspectrum E_m. Here, we study the scaling behavior of the eigenspectrum by analyzing the Hausdorff dimension. An elaborate discussion will be provided in the following section. In addition, the scaling nature of the eigenstates is done by studying the multifractal analysis. Classification of the eigenstates, such as localized, extended, or critical states, can be performed by computing the inverse participation ratio (IPR). The IPR of the mth eigenstate is defined as

$$
\text{IPR}^{(m)} = \sum_{i=1}^{L} \left| \phi_i^{(m)} \right|^4. \tag{3}
$$

Since an IPR value is not sufficient to describe the underlying physics of an eigenstate associated with the critical nature, the higher moment of the IPR is more fundamental in that case. Therefore, a multifractal nature of the eigenstates can be identified through the generalized IPR and its scaling exponent τ_q [32,45,50] using the relation

$$
\text{IPR}_q^{(m)} = \sum_{i=1}^{L} \left| \phi_i^{(m)} \right|^{2q} \rightarrow L^{-\tau_q}, \tag{4}
$$

where τ_q is also known as the mass exponent and q is a real number. The mass exponent vanishes for the localized states, whereas it varies linearly with the system dimension d for the delocalized state as $\tau_q = d(q-1)$. Furthermore, the scaling exponents of the multifractal states can be characterized by a nonlinear relation where d (see above) is no longer an integer and further acquire q dependence, which can be written as

$$
\tau_q = D_q(q-1), \tag{5}
$$

where D_q denotes the fractal dimension of the eigenstates. Therefore, an extended state and a localized state have, respectively, 1 and 0 as their fractal dimensions, while an intermediate value of D_q (between 1 and 0) denotes the fractal nature of the eigenstates.

In general, localization in a disordered system can also be characterized by using the normalized participation ratio (NPR), which for the mth eigenstate is defined as

$$
\text{NPR}^{(m)} = \left[L \sum_{i=1}^{L} \left| \phi_i^{(m)} \right|^4 \right]^{-1} = \frac{\text{PR}^{(m)}}{L}, \tag{6}
$$

where L is the system size and PR is the participation ratio. In the extended regime, PR grows linearly with system size L, while it vanishes in the localized regime in the thermodynamic limit. For further analysis, we consider the average value of

the NPR. Using the averaged NPR values, we can identify the order parameter for the localization transition as

$$\sigma = \sqrt{\frac{\text{PR}}{L}} = \sqrt{\text{NPR}}. \tag{7}$$

In the vicinity of the phase transition, the observables display power law behavior, with their critical exponents behaving as [51]

$$\sigma \sim (-\varepsilon)^{\beta}, \quad \text{PR} \sim \varepsilon^{-\gamma}, \quad \xi \sim |\varepsilon|^{-\nu}. \tag{8}$$

Here, $\varepsilon = (\lambda - \lambda_c)/\lambda_c$ is the reduced disorder potential strength, with λ_c being the critical disorder strength for the localization transitions, and ξ is the correlation (or localization) length. β, γ, and ν are the order parameter exponent, the participation ratio exponent, and the correlation length exponent, respectively.

Following Ref. [51], the order parameter σ associated with two different system sizes yields a function $R[L, L']$, which is given by

$$R[L, L'] = \frac{\ln\left(\sigma_L^2 / \sigma_{L'}^2\right)}{\ln(L/L')} + 1. \tag{9}$$

The critical point for the transition λ_c and the critical exponent ratio γ/ν are determined using the above two-system size-variable function $R[L, L']$. The curves corresponding to $R[L, L']$ as a function of the strength of the potential in the vicinity of the critical point for several pairs of the system of sizes L and L' intersect each other at a common fixed point. The critical potential strength λ_c and the exponent ratio γ/ν are determined from the abscissa and the ordinate of the common crossing point, respectively.

In the vicinity of the critical point, a finite-size scaling form of the order parameter σ for a finite system is defined by

$$\sigma = L^{-\beta/\nu} F(\varepsilon L^{1/\nu}), \tag{10}$$

where F is a scaling function. Similarly, a finite-size scaling form of the PR for a finite-size system is defined by

$$\text{PR} = L^{\gamma/\nu} G(\varepsilon L^{1/\nu}), \tag{11}$$

where G is another scaling function. Using Eq. (7), Eq. (11) can be rewritten as

$$\sigma^2 L = L^{\gamma/\nu} G(\varepsilon L^{1/\nu}), \tag{12}$$

which can be further expressed as

$$\sigma^2 = L^{\gamma/\nu - 1} G(\varepsilon L^{1/\nu}). \tag{13}$$

Hence, a plot of $\sigma^2 L^{1-\gamma/\nu}$ versus $\varepsilon L^{1/\nu}$ for different system sizes L should fall onto a single curve denoted by $G(\varepsilon L^{1/\nu})$ if the critical potential strength λ_c and the critical exponents are correctly determined. In the following we will utilize the above prescription to study the critical properties of the reentrant localization transitions.

III. RESULTS

The localization properties of the model shown in Eq. (1) were discussed in detail in Ref. [49]. It was shown that the system exhibits a reentrant localization transition in the limit of staggered disorder, i.e., $\lambda_A = -\lambda_B = \lambda$, which is depicted
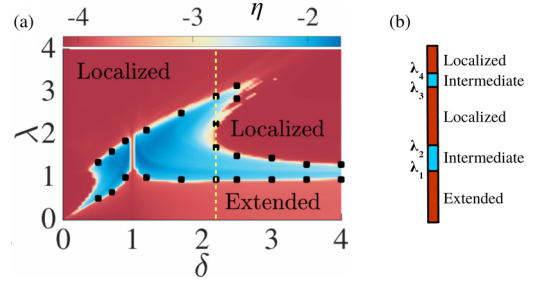

FIG. 1. The phase diagram is plotted as a function of hopping dimerization δ and disorder strength λ in (a). In (b), a schematic picture of the series of transitions is shown for $\delta = 2.2$ [marked by the dashed line in (a)] [49].

as a phase diagram in the δ-λ plane in Fig. 1 (see Ref. [49] for details). Note that the phase diagram shown in Fig. 1(a) was obtained by utilizing the behavior of the average participation ratios, such as the average inverse and normalized participation ratios, as a function of λ. Here, IPR and NPR are calculated by taking the average over all the eigenstates corresponding to the Hamiltonian shown in Eq. (1) [49], and they are given by

$$\text{IPR} = \frac{1}{m} \sum_m \text{IPR}^{(m)},$$

$$\text{NPR} = \frac{1}{m} \sum_m \text{NPR}^{(m)}. \tag{14}$$

The different phases in the phase diagram are computed using a quantity η [49,52] which is defined as

$$\eta = \log_{10}(\text{IPR} \times \text{NPR}). \tag{15}$$

In the phase diagram in Fig. 1(a), the red regions correspond to the extended and localized phases, and the central blue region bounded by the dark symbols is the intermediate phase. It can be seen from the phase diagram that for a range of values of δ, the system undergoes two localization transitions as a function of λ, indicating the reentrant localization transition. Although the reentrant localization is feasible in both regimes of hopping dimerization corresponding to $\delta < 1$ and $\delta > 1$ [49], for our discussion we restrict ourselves to the regime of $\delta > 1$ for concreteness. For our analysis, we explore the critical properties of a cut through the phase diagram along the y axis at $\delta = 2.2$ [dashed yellow line in Fig. 1(a)]. As λ is increased, the system as a whole undergoes two localization transitions through two intermediate phases exhibiting a series of transitions from extended to intermediate to localized to intermediate to localized phases occurring at four critical points, λ_1, λ_2, λ_3, and λ_4, as schematically depicted in Fig. 1(b). In the following our focus is on studying the fractal nature of the eigenstates and eigenspectra across these transitions and determining the transition points through a finite-size scaling analysis.

A. Multifractal analysis

As already discussed in the previous section, the two localization transitions in this case occur through two intermediate regions. In analogy with the direct localization transition in
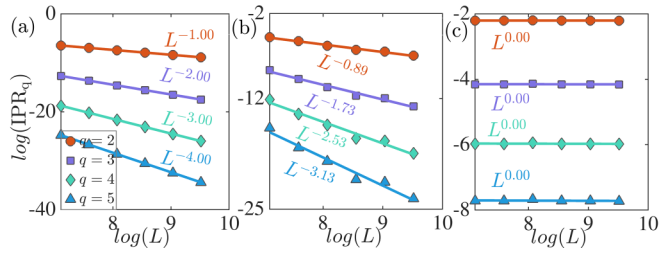
FIG. 2. The generalized IPR is plotted as a function of different system sizes L corresponding to different moments of the intensity q. The slopes of the curves are characterized by the mass exponent τ_q. We show three distinguishing behaviors of τ_q by considering the potential strength λ in the extended, multifractal, and localized regions in (a), (b), and (c), respectively. We consider $\lambda = 0.5$ and eigenstate index $m/L = 0.5$ in (a), $\lambda = 0.903$ (first critical point) and eigenstate index $m/L = 0.1$ in (b), and $\lambda = 4$ and eigenstate index $m/L = 0.5$ in (c). For all cases, we take $\delta = 2.2$.

the case of the AA model and other models in which the localization transition occurs through an intermediate region, we expect the existence of multifractal eigenstates in the intermediate phases. Thus, to explore deeper into the nature of the states in different regions we perform a multifractal analysis [32,45] of the eigenstates and calculate the associated fractal dimensions to arrive at an intuitive picture of the critical regions.

In our analysis, by following Eqs. (4) and (5), we first obtain the correlation dimension, denoted by D_2, corresponding to $q = 2$, from the relation

$$\mathrm{IPR}_2^n \propto L^{-D_2}. \tag{16}$$

D_2 can be obtained as the slope of the $\log(\mathrm{IPR}_2)$ versus $\log(L)$ plot corresponding to different states, as shown in Fig. 2 (red circles). Furthermore, in order to gain insights into the variation of D_2 over the entire spectrum, we plot D_2 as a function of the eigenstate index and λ at $\delta = 2.2$ in Fig. 3, which clearly shows the existence of the extended, localized, and multifractal states. While the expected reentrant feature can be seen in Fig. 3, a clear understanding of this can be obtained from the structure of the eigenstates. In this regard, we plot the eigenstates for different values of λ, namely, $\lambda = 1.0, 1.5, 2.0, 2.5,$ and 3.5 for a particular
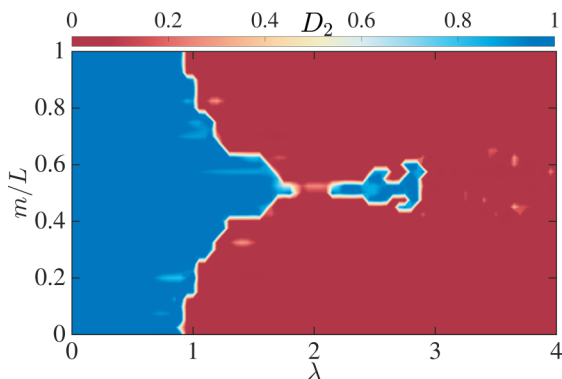
eigenstate with index $m/L = 0.5$ as a function of the site index i in Figs. 4(a)–4(e). It is observed that the wave functions at $\lambda = 1.0$ and $\lambda = 1.5$ spread uniformly over the entire lattice, indicating their extended nature. Further, a localized state is observed at $\lambda = 2.0$. However, at $\lambda = 2.5$, the extended character reemerges, and finally, as expected, the wave function becomes completely localized at $\lambda = 3.5$. As a further check, we plot the eigenstates corresponding to identical values of λ ($\lambda = 1.0, 1.5, 2.0, 2.5,$ and 3.5) for another dimerization strength, $\delta = 1.5$, as a function of site index i in Figs. 4(f)–4(j), where the reentrant behavior is absent.

To complement the above analysis to distinguish the nature of the states, we compute the average values of D_2 over the eigenstates. In Fig. 5(a), we plot D_2^{avg} as a function of λ, where the extended and localized phases are characterized by $D_2^{\mathrm{avg}} = 1$ and 0, respectively. Here, $0 < D_2^{\mathrm{avg}} < 1$ implies the presence of states that are multifractal in nature. The average value of D_2 is calculated by considering some of the states from the middle of the spectrum. In addition, we also examine the variation of the exponents by considering different values of $q > 2$ ($q = 3, 4, 5$) that correspond to higher moments of the eigenstates. We obtain signatures which exactly match the natures of the extended, multifractal, and localized states
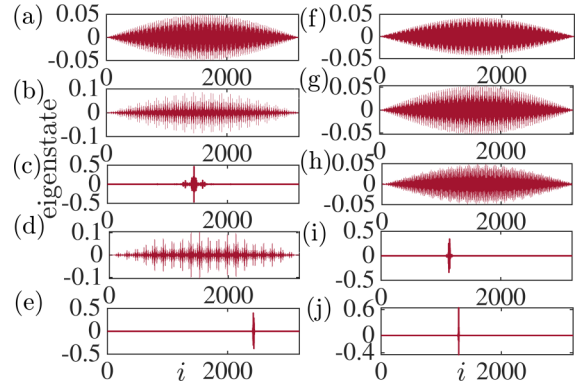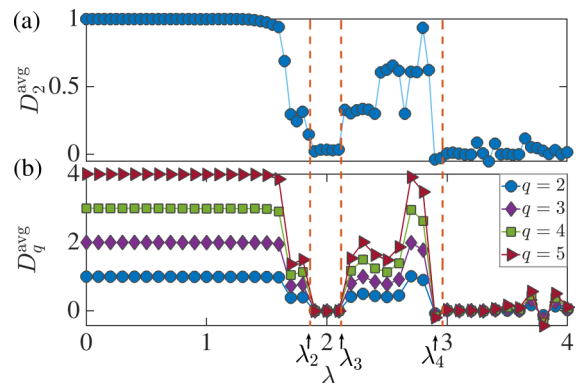

FIG. 4. (a)–(e) show the eigenstates as a function of site index i corresponding to $\lambda = 1.0, 1.5, 2.0, 2.5,$ and 3.5 for the eigenstate index ($m/L = 0.5$) and $\delta = 2.2$. As a comparison, (f)–(j) represent the eigenstate behavior corresponding to $\delta = 1.5$ and $m/L = 0.5$. The system size taken for the calculation is $L = 3194$.

FIG. 3. The values of D_2 as a function of λ and eigenstate index (m/L) are plotted for $\delta = 2.2$.

FIG. 5. D_2^{avg} and D_q^{avg} are plotted as a function of λ in (a) and (b), respectively, for $\delta = 2.2$.
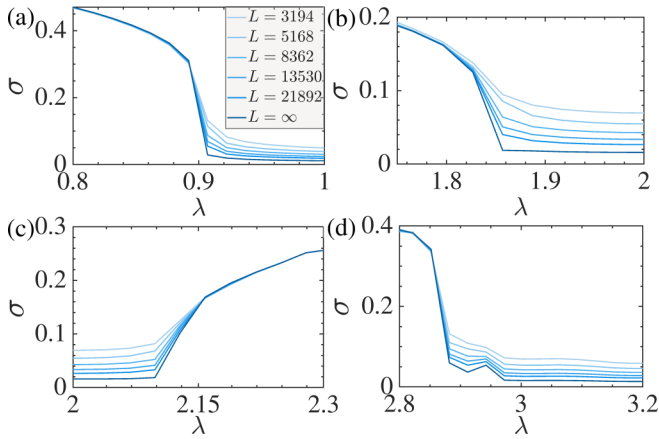
FIG. 6. The order parameter σ is plotted as a function of λ corresponding to four different critical transition points, λ_1, λ_2, λ_3, and λ_4. We consider states within a narrow band with indices $(m/L) = [0$ to $0.05]$, $[0.45$ to $0.5]$, $[0.45$ to $0.5]$, and $[0.45$ to $0.5]$ for the calculation of σ in (a)–(d), respectively. Light to dark curves correspond to small to large system sizes. The curve with deep blue color is obtained by using finite-size extrapolation.

of the spectrum, as shown in Figs. 2(a)–2(c), respectively. A clear understanding of these features can also be achieved by plotting D_q^{avg} for the entire range of λ. In Fig. 5(b), we plot D_q^{avg} as a function of λ for $q = 2$, 3, 4, and 5. The q dependence of D_q^{avg} indicates the presence of multifractal states. In Fig. 5, different transitions are marked by the vertical dashed lines.

B. Critical state analysis

In this section, we establish the transition points by analyzing the behavior of σ which is directly related to the NPR of the states. From the definition, σ for different lengths should approach zero at the localization transition. Therefore, it will be possible to estimate all the critical points by using the finite-size extrapolation of σ. For this purpose, we compute σ by considering the eigenstates in a narrow band near the approximate transition boundaries. The choice of a narrow band is due to the presence of the ME for which the transition occurs at different critical λ for different states. We plot σ for different system sizes, namely, $L = 3194$, 5168, 8362, 13 530, and 21 892 as a function of λ in Figs. 6(a)–6(d) across the transition points λ_1, λ_2, λ_3, and λ_4, respectively. A finite-size extrapolation reveals that for all cases, σ in the limit of $L \to \infty$ falls to a minimum after a critical λ for different transitions. As an example we show a finite-size scaling analysis of σ corresponding to several values of $\lambda = 0.8$, 0.85, 0.9, 0.95, and 1.0 across the first critical point in Fig. 7. The extrapolated values of σ tending to zero for larger values of λ clearly indicate a localization transition. This analysis defines the relevant range of λ for our exploration of the critical properties. Once the limits of λ around the critical transition points are identified, we use them to calculate the function $R[L, L']$ [see Eq. (9)].

We first focus on the first localization transition, which involves two critical points, such as λ_1 and λ_2, corresponding
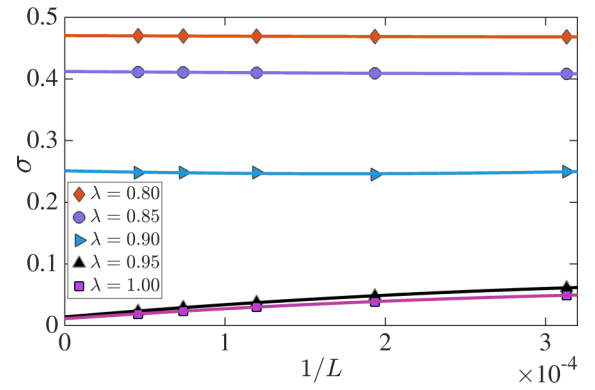

FIG. 7. The finite-size scaling analysis is shown for several values of λ. The system sizes are $L = 3194$, 5168, 8362, 13 530, and 21 892.

to the extended-intermediate and intermediate-localized transitions. Like in the case for σ, for our analysis, to compute the function $R[L, L']$ we use the eigenstates corresponding to a narrow band of the spectrum. We plot $R[L, L']$ as a function of λ for both transitions around λ_1 and λ_2 in Figs. 8(a) and 8(b), respectively. The crossing of all the curves at a single point in both Figs. 8(a) and 8(b) allows us to obtain the critical points as $\lambda_1 = 0.903$ and $\lambda_2 = 1.836$. As already mentioned in Sec. II, following Eq. (12), curves of $\sigma^2 L^{1-\gamma/\nu}$ versus $\varepsilon L^{1/\nu}$ for different system sizes, $L = 8362$, 13 530, 21 892, and 35 422, collapse with the estimated critical strength $\lambda_1 = 0.903$. A perfect data collapse is obtained by considering $\gamma/\nu = 0.83 \pm 0.05$ and $\nu = 1.8$ for $\lambda_1 = 0.903$, as shown in the inset in Fig. 8(a). Similarly, for the second critical point ($\lambda_2 = 1.836$), a perfect data collapse is obtained by setting $\gamma/\nu = 0.77 \pm 0.04$ and $\nu = 1.7$ [inset of Fig. 8(b)]. Note that the γ/ν considered for the data collapse matches fairly well the ordinate corresponding to the points of intersection of $R[L, L']$ as a function of λ in Figs. 8(a) and 8(b).

We now turn our focus to the second localization transition through the second critical region as depicted in Fig. 1. This involves two transitions, namely, localized-intermediate and intermediate-localized transitions at critical points λ_3 and λ_4, respectively. Following a scaling hypothesis similar to that above, for the localized-intermediate transition, we obtain the crossing of $R[L, L']$ data at a single point, as depicted in Fig. 8(c), resulting in a value of $\lambda_3 = 2.127$. Further, by using the value of λ_3, a perfect data collapse is achieved in the $\sigma^2 L^{1-\gamma/\nu}$ versus $\varepsilon L^{1/\nu}$ plot by setting $\gamma/\nu = 0.79 \pm 0.03$ and $\nu = 1.7$, as shown in the inset of Fig. 8(c). This suggests that the two transitions occurring at λ_2 and λ_3 corresponding to the transitions to and from the first localized phase (intermediate-localized and localized-intermediate) belong to the same universality class.

It is now expected that the transition to the second localized phase, i.e., the fourth transition occurring at λ_4, falls in the same universality class as that of the second and third transitions observed at λ_2 and λ_3. However, in our scaling analysis, we find an anomalous scaling behavior of $R[L, L']$, which is why we have failed to achieve an accurate critical point λ_4 and the associated exponents (see Fig. 9). The actual reason for
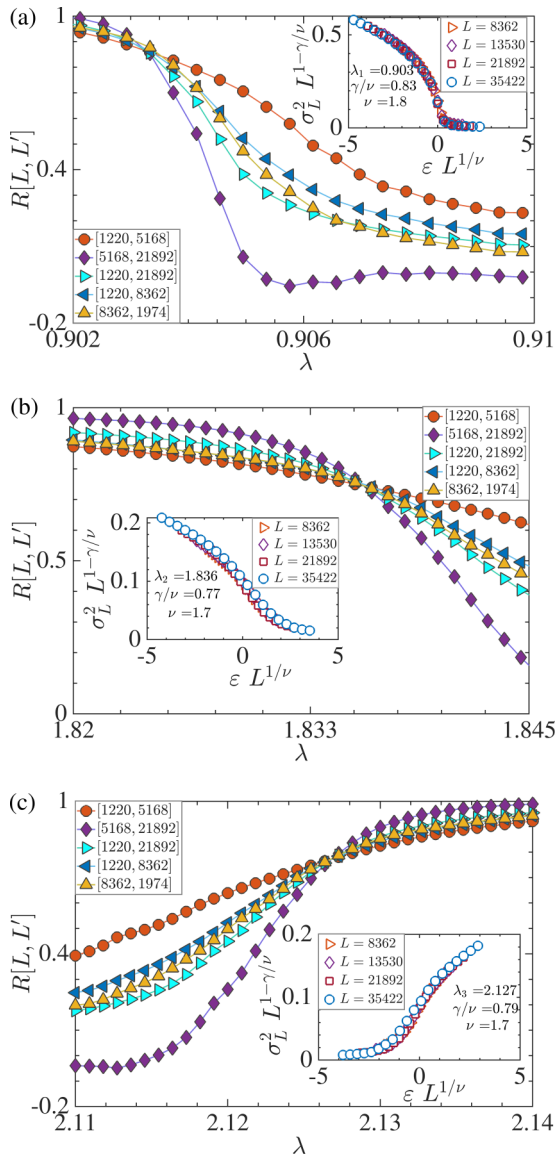
FIG. 8. Shown are plots of $R[L, L']$ in the vicinity of the first critical quasiperiodic potential strength λ_1 in (a), the second critical quasiperiodic potential strength λ_2 in (b), and third critical quasiperiodic potential strength λ_3 in (c), corresponding to $\delta = 2.2$. The insets show the data collapse with the σ^2 data in the vicinity of the first, second, and third critical points. Good data collapse is observed for all the transition points. The existence of single universal scaling functions can easily be inferred from the data collapse. We have done the calculations by taking an average over the states in the band with indices $m/L = [0 \text{ to } 0.05]$ for the first critical point and the states in the band with indices $m/L = [0.45 \text{ to } 0.5]$ for the second and third critical points of the energy spectrum in this study.

this behavior can be attributed to the anomalous distribution of the extended state (NPR $\neq$ 0) near the transition.

Furthermore, we reconfirm that the critical exponents from the scaling relation of PR_L, which denotes the participation ratio corresponding to different system sizes using Eq. (8), can be written as $PR_L \sim L^{\gamma/\nu}$. From this relation, a plot of $\log(PR_L)$ versus $\log(L)$ for different lengths L at the critical point should result in a straight line with slope γ/ν. We per-
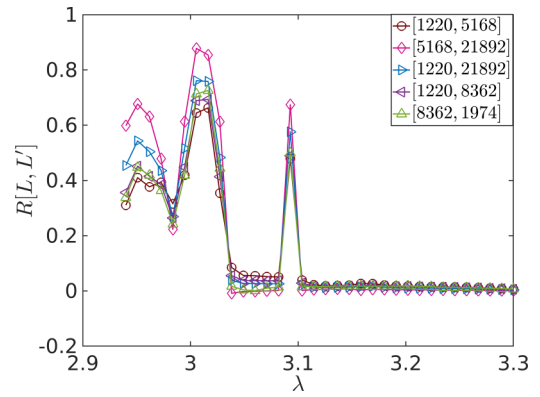

FIG. 9. The functions $R[L, L']$ are plotted as a function of λ in the vicinity of the fourth critical point λ_4 at $\delta = 2.2$. We have done the calculations by taking an average over the states in the band with indices $m/L = [0.45 \text{ to } 0.5]$ of the energy spectrum in this study.

form this analysis at all three critical points, λ_1, λ_2, and λ_3, in Fig. 10 and obtain values of γ/ν of 0.83 ± 0.05, 0.77 ± 0.04, and 0.79 ± 0.03, respectively. The exponents obtained in our analysis should satisfy a hyperscaling law expressed as [51]

$$\frac{2\beta}{\nu} + \frac{\gamma}{\nu} = 1. \qquad (17)$$

Using the hyperscaling relation given in Eq. (17), it is possible to extract another ratio of the exponents, i.e., β/ν, via

$$\frac{\beta}{\nu} = \frac{1}{2}\left(1 - \frac{\gamma}{\nu}\right). \qquad (18)$$

Since at the critical point $\xi = L$, from Eq. (8) we have $\sigma_L \sim L^{-\beta/\nu}$. In order to establish the hyperscaling relation we plot $\log(\sigma_L)$ as a function of $\log(L)$ for different system sizes corresponding to critical points λ_1, λ_2, and λ_3 in Fig. 11. The slopes of the curves yield the exponent ratios $\beta/\nu = 0.086 \pm 0.03$, 0.116 ± 0.02, and 0.1 ± 0.02 for $\lambda_1 = 0.903$, $\lambda_2 = 1.836$, and $\lambda_3 = 2.127$, respectively. These values of the exponent ratios γ/ν (0.83, 0.77, and 0.79) and β/ν (0.086, 0.116, and 0.100) clearly satisfy the hyperscaling relation [Eq. (17)] at the critical points.
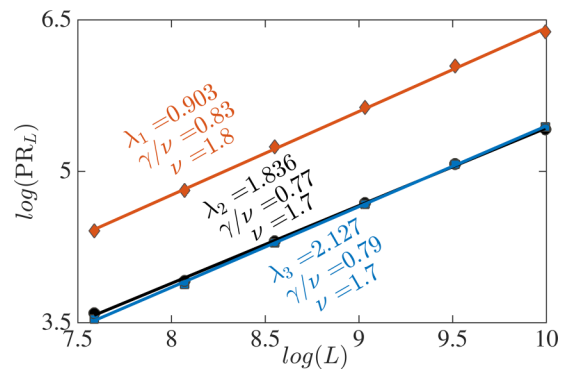

FIG. 10. The exponent ratio γ/ν is calculated by plotting $\ln(PR_L)$ as a function of $\ln(L)$ for different system sizes $L = 1974, 3194, 5168, 8362, 13\,530, 21\,892$ corresponding to three different critical points, λ_1, λ_2, and λ_3.
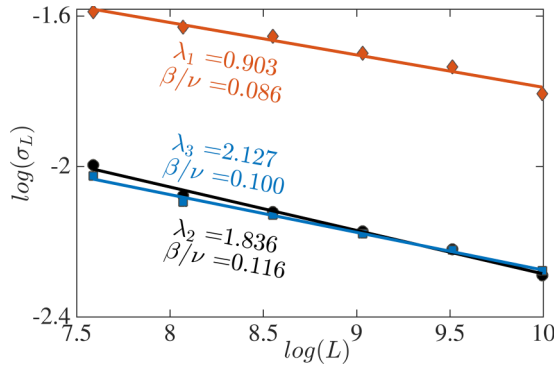
FIG. 11. The exponent ratio β/ν is calculated by plotting the order parameter σ_L as a function of different system lengths L corresponding to three different critical potential strengths, namely, λ_1, λ_2, and λ_3.

C. Hausdorff dimension

The understanding of the details of the energy spectrum at the critical regime can be complemented by computing the Hausdorff dimension of the system. A direct box-counting method is applied for this analysis [31]. Consider the total number of boxes N_l for a given box length l such that N_l spans the entire energy spectrum. N_l shows a power law behavior with l as

$$N_l \propto l^{-D_H}, \tag{19}$$

where D_H denotes the Hausdorff dimension corresponding to the energy spectrum. In our case, we compute D_H by following Eq. (19) in two different critical regions corresponding to $\lambda = 1.2$ and 2.5, which respectively denote the first and second intermediate regimes. In Fig. 12, we plot N_l as a function of l, which exhibits a power law behavior with the exponent $D_H = 0.61$ (blue squares) and 0.85 (green diamonds) for $\lambda = 1.2$ (first intermediate regime) and 2.5 (second intermediate regime), respectively. For comparison, we plot the corresponding AA limit ($\delta = 1$, $\lambda_A = \lambda_B = \lambda = 2$; red circles), which yields $D_H = 0.5$ [53]. We identify the former case as "DIM" and the latter case as "AA." From the analysis, it is realized that the Hausdorff dimension, in this case, is different from the standard AA model. At the transition point of the AA model, all the eigenstates are critical in nature. However, the eigenstates possess a mixture of localized and extended features for the DIM model, thereby resulting in a larger value of the Hausdorff dimension D_H compared to that
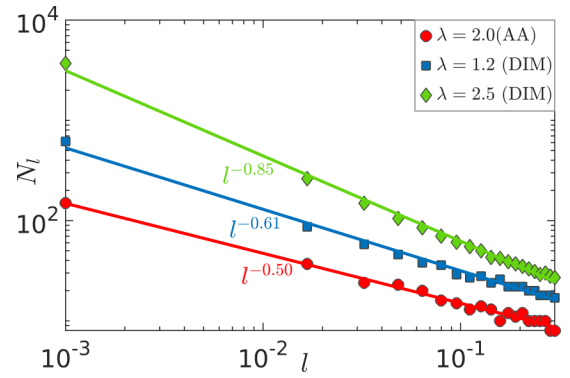

FIG. 12. N_l is shown as a function of box length l in the log-log scale corresponding to $\lambda = 1.2$ (blue squares) and $\lambda = 2.5$ (green diamonds). We identify these two cases as "DIM," and the corresponding chosen $\delta = 2.2$. For comparison, we show the result for the pure AA limit ($\delta = 1$, red circles). The slopes of these plots give the Hausdorff dimensions, which are obtained as $D_H = 0.61$ and 0.85 for $\lambda = 1.2$ and 2.5, respectively. Note that for the AA model $D_H = 0.5$. The system size considered for the calculation is $L = 13\,530$.

of the AA model. Hence, we conclude that the spectrum of the DIM model is denser than that of the AA model.

IV. CONCLUSION

A one-dimensional quasiperiodic lattice model in the presence of hopping dimerization and a staggered on-site quasiperiodic potential exhibits reentrant localization transitions. The transitions occur for a range of dimerization strengths through two intermediate phases, resulting in four critical points. In this work, we performed a multifractal analysis of the eigenstates and found that the states within the intermediate phases are multifractal in nature. Further, we characterized these transition points by using appropriate finite-size scaling laws for different order parameters. We also obtained the associated critical exponents, which were found to obey the hyperscaling laws. We also observed that the second (intermediate-localized) and third (localized-intermediate) phase transitions belong to the same universality class. Note that while we are able to accurately determine the first three critical points associated with the first localization transition, we fail to determine the last critical point of the transition to the second localized phase. Finally, we calculated the Hausdorff dimensions in the two critical regions, which were found to be different from the standard AA limit.

[1] P. W. Anderson, Phys. Rev. **109**, 1492 (1958).

[2] E. Abrahams, P. W. Anderson, D. C. Licciardello, and T. V. Ramakrishnan, Phys. Rev. Lett. **42**, 673 (1979).

[3] J. Sokoloff, Phys. Rep. **126**, 189 (1985).

[4] D. R. Grempel, S. Fishman, and R. E. Prange, Phys. Rev. Lett. **49**, 833 (1982).

[5] B. Simon, Ann. Phys. (NY) **159**, 157 (1985).

[6] M. Kohmoto, Phys. Rev. Lett. **51**, 1198 (1983).

[7] S. Ostlund, R. Pandit, D. Rand, H. J. Schellnhuber, and E. D. Siggia, Phys. Rev. Lett. **50**, 1873 (1983).

[8] S. Aubry and G. André, Ann. Israel Phys. Soc. **3**, 18 (1980).

[9] Y. Lahini, R. Pugatch, F. Pozzi, M. Sorel, R. Morandotti, N. Davidson, and Y. Silberberg, Phys. Rev. Lett. **103**, 013901 (2009).

[10] R. Merlin, K. Bajema, R. Clarke, F. Y. Juang, and P. K. Bhattacharya, Phys. Rev. Lett. **55**, 1768 (1985).

[11] D. Tanese, E. Gurevich, F. Baboux, T. Jacqmin, A. Lemaître, E. Galopin, I. Sagnes, A. Amo, J. Bloch, and E. Akkermans, Phys. Rev. Lett. **112**, 146404 (2014).

[12] P. Roushan, C. Neil, J. Tangpanitanon, V. M. Bastidas, A. Megrant, R. Barends, Y. Chen, Z. Chen, B. Chiaro, A. Dunsworth, A. Fowler, B. Foxen, M. Giustina, E. Jeffrey, J. Kelly, E. Lucero, J. Mutus, M. Neeley, C. Quintana, D. Sank, A. Vainsencher, J. Wenner, T. White, H. Neven, D. G. Angelakis, and J. Martinis, Science **358**, 1175 (2017).

[13] J. Billy, V. Josse, Z. Zuo, A. Bernard, B. Hambrecht, P. Lugan, D. Clément, L. Sanchez-Palencia, P. Bouyer, and A. Aspect, Nature (London) **453**, 891 (2008).

[14] A. Aspect and M. Inguscio, Phys. Today **62**(8), 30 (2009).

[15] Y. Lahini, A. Avidan, F. Pozzi, M. Sorel, R. Morandotti, D. N. Christodoulides, and Y. Silberberg, Phys. Rev. Lett. **100**, 013906 (2008).

[16] H. P. Lüschen, S. Scherg, T. Kohlert, M. Schreiber, P. Bordia, X. Li, S. Das Sarma, and I. Bloch, Phys. Rev. Lett. **120**, 160404 (2018).

[17] L. Fallani, J. E. Lye, V. Guarrera, C. Fort, and M. Inguscio, Phys. Rev. Lett. **98**, 130404 (2007).

[18] G. Roux, T. Barthel, I. P. McCulloch, C. Kollath, U. Schollwöck, and T. Giamarchi, Phys. Rev. A **78**, 023628 (2008).

[19] C. D'Errico, E. Lucioni, L. Tanzi, L. Gori, G. Roux, I. P. McCulloch, T. Giamarchi, M. Inguscio, and G. Modugno, Phys. Rev. Lett. **113**, 095301 (2014).

[20] H. Yao, T. Giamarchi, and L. Sanchez-Palencia, Phys. Rev. Lett. **125**, 060401 (2020).

[21] M. Sbroscia, K. Viebahn, E. Carter, J.-C. Yu, A. Gaunt, and U. Schneider, Phys. Rev. Lett. **125**, 200604 (2020).

[22] L. Sanchez-Palencia and L. Santos, Phys. Rev. A **72**, 053607 (2005).

[23] K. Viebahn, M. Sbroscia, E. Carter, J.-C. Yu, and U. Schneider, Phys. Rev. Lett. **122**, 110404 (2019).

[24] S. Iyer, V. Oganesyan, G. Refael, and D. A. Huse, Phys. Rev. B **87**, 134202 (2013).

[25] H. P. Lüschen, P. Bordia, S. Scherg, F. Alet, E. Altman, U. Schneider, and I. Bloch, Phys. Rev. Lett. **119**, 260401 (2017).

[26] P. Bordia, H. Lüschen, S. Scherg, S. Gopalakrishnan, M. Knap, U. Schneider, and I. Bloch, Phys. Rev. X **7**, 041047 (2017).

[27] C. M. Soukoulis and E. N. Economou, Phys. Rev. Lett. **48**, 1043 (1982).

[28] F. A. An, E. J. Meier, and B. Gadway, Phys. Rev. X **8**, 031045 (2018).

[29] J. D. Bodyfelt, D. Leykam, C. Danieli, X. Yu, and S. Flach, Phys. Rev. Lett. **113**, 236403 (2014).

[30] Y. Wang, X. Xia, L. Zhang, H. Yao, S. Chen, J. You, Q. Zhou, and X.-J. Liu, Phys. Rev. Lett. **125**, 196604 (2020).

[31] H. Yao, H. Khoudli, L. Bresque, and L. Sanchez-Palencia, Phys. Rev. Lett. **123**, 070405 (2019).

[32] X. Deng, S. Ray, S. Sinha, G. V. Shlyapnikov, and L. Santos, Phys. Rev. Lett. **123**, 025301 (2019).

[33] S. Das Sarma, S. He, and X. C. Xie, Phys. Rev. B **41**, 5544 (1990).

[34] J. Biddle, B. Wang, D. J. Priour, and S. Das Sarma, Phys. Rev. A **80**, 021603(R) (2009).

[35] J. Biddle and S. Das Sarma, Phys. Rev. Lett. **104**, 070601 (2010).

[36] J. Biddle, D. J. Priour, B. Wang, and S. Das Sarma, Phys. Rev. B **83**, 075105 (2011).

[37] S. Ganeshan, J. H. Pixley, and S. Das Sarma, Phys. Rev. Lett. **114**, 146601 (2015).

[38] F. A. An, K. Padavić, E. J. Meier, S. Hegde, S. Ganeshan, J. H. Pixley, S. Vishveshwara, and B. Gadway, Phys. Rev. Lett. **126**, 040603 (2021).

[39] S. Roy, S. Mukerjee, and M. Kulkarni, Phys. Rev. B **103**, 184203 (2021).

[40] A. P. Siebesma and L. Pietronero, Europhys. Lett. **4**, 597 (1987).

[41] M. Kohmoto, L. P. Kadanoff, and C. Tang, Phys. Rev. Lett. **50**, 1870 (1983).

[42] A. Szabó and U. Schneider, Phys. Rev. B **98**, 134201 (2018).

[43] J. H. Han, D. J. Thouless, H. Hiramoto, and M. Kohmoto, Phys. Rev. B **50**, 11365 (1994).

[44] X. Li, X. Li, and S. Das Sarma, Phys. Rev. B **96**, 085119 (2017).

[45] S. Roy, I. M. Khaymovich, A. Das, and R. Moessner, SciPost Phys. **4**, 025 (2018).

[46] C. Tang and M. Kohmoto, Phys. Rev. B **34**, 2041 (1986).

[47] M. Kohmoto, B. Sutherland, and C. Tang, Phys. Rev. B **35**, 1020 (1987).

[48] A. Purkayastha, A. Dhar, and M. Kulkarni, Phys. Rev. B **96**, 180204(R) (2017).

[49] S. Roy, T. Mishra, B. Tanatar, and S. Basu, Phys. Rev. Lett. **126**, 106803 (2021).

[50] F. Evers and A. D. Mirlin, Rev. Mod. Phys. **80**, 1355 (2008).

[51] Y. Hashimoto, K. Niizeki, and Y. Okabe, J. Phys. A **25**, 5211 (1992).

[52] X. Li and S. Das Sarma, Phys. Rev. B **101**, 064203 (2020).

[53] K. Ikezawa and M. Kohmoto, J. Phys. Soc. Jpn. **63**, 2261 (1994).